Neurobiology of Aging 75 (2019) 25–37

Contents lists available at ScienceDirect

Neurobiology of Aging

journal homepage: www.elsevier.com/locate/neuaging

Age-dependent behavioral and biochemical characterization of single APP knock-in mouse ($APP^{NL-G-F/NL-G-F}$) model of Alzheimer's disease

Jogender Mehla [a], Sean G. Lacoursiere [a], Valerie Lapointe [a], Bruce L. McNaughton [a,b], Robert J. Sutherland [a], Robert J. McDonald [a,**], Majid H. Mohajerani [a,*]

[a] Canadian Center for Behavioural Neuroscience, University of Lethbridge, Lethbridge, Alberta, Canada
[b] Center for the Neurobiology of Learning and Memory, University of California at Irvine, Irvine, CA, USA

ARTICLE INFO

Article history:
Received 12 July 2018
Received in revised form 22 October 2018
Accepted 28 October 2018
Available online 5 November 2018

Keywords:
Alzheimer's disease
APP^{NL-G-F} mice
Learning and memory
Amyloid-β
Choline acetyltransferase
Tyrosine hydroxylase

ABSTRACT

Saito et al developed a novel amyloid precursor protein (APP) knock-in mouse model (APP^{NL-G-F}) for Alzheimer's disease (AD) to overcome the problem of overexpression of APP in available transgenic mouse models. However, this new mouse model for AD is not fully characterized age-dependently with respect to behavioral and biochemical changes. Therefore, in the present study, we performed an age-dependent behavioral and biochemical characterization of this newly developed mouse model. Here, we used 3-, 6-, 9-, and 12-month-old APP^{NL-G-F} and C57BL/6J mice. We used a separate cohort of animals at each age point. Morris water maze, object recognition, and fear-conditioning tests were used for the assessment of learning and memory functions and open-field test to measure the general locomotor activity of mice. After each testing point, we perfused the mice and collected the brain for immunostaining. We performed the immunostaining for amyloid burden (4G8), glial fibrillary acidic protein, choline acetyltransferase, and tyrosine hydroxylase. The results of the present study indicate that APP^{NL-G-F} mice showed age-dependent memory impairments with maximum impairment at the age of 12 months. These mice showed memory impairment in Morris water maze and fear conditioning tests when they were 6 months old, whereas, in object recognition test, memory deficit was found in 9-month-old mice. APP^{NL-G-F} mice age dependently showed an increase in amyloid load in different brain regions. However, no amyloid pathology was found in 3-month-old APP^{NL-G-F} mice. Choline acetyltransferase neurons in medial septum-diagonal band complex and tyrosine hydroxylase neurons in locus coeruleus were decreased significantly in APP^{NL-G-F} mice. This mouse model also indicated an age-dependent increase in glial fibrillary acidic protein load. It can be concluded from the results that the APP^{NL-G-F} mouse model may be used to explore the Aβ hypothesis, molecular, and cellular mechanisms involved in AD pathology and to screen the therapeutic potential compounds for the treatment of AD.

1. Introduction

Alzheimer's disease (AD), the commonest form of dementia, is pathologically characterized by deposition of amyloid-β (Aβ) plaques and formation of neurofibrillary tangles in the brain (Ettcheto et al., 2017; Hardy and Selkoe, 2002). The sporadic form of AD (SAD) is the most common form, which accounts for ~85% of cases (Ettcheto et al., 2018; Gidyk et al., 2015). The SAD has a complex etiology, and the pathology and resulting behavioral consequences associated with SAD are heterogeneous (McDonald, 2002; McDonald et al., 2010; Santos et al., 2017). Worldwide, approximately 47 million people suffer from AD (Sasaguri et al., 2017). AD is a chronic neurodegenerative disease which is often responsible for cognitive dysfunctions in the elderly (Bateman et al., 2012). The deposition of Aβ plaque and formation of neurofibrillary tangles lead to atrophy, synaptic and neuronal loss, and gliosis in the brain. As the disease progresses, patients with AD develop several symptoms including, memory loss, difficulties with performing routine task, depression, hallucination, anxiety, delusion, agitation, and aggression (de Vugt et al., 2005; Ferri et al., 2004). In addition, a decreased level of the neurotransmitter acetylcholine and the enzyme choline acetyltransferase (ChAT) has been reported in the postmortem brain of the patients with AD (Gil-

* Corresponding author at: Canadian Center for Bahavioural Neuroscience, University of Lethbridge, 4401 University Drive Lethbridge, Alberta T1K 3M4, Canada. Tel.: (403) 394-3950; Fax: 403 329 2775.
** Corresponding author at: Canadian Center for Bahavioural Neuroscience, University of Lethbridge, 4401 University Drive Lethbridge, Alberta T1K 3M4, Canada. Tel.: (403) 394-3983; Fax: 403 329 2775.
E-mail addresses: r.mcdonald@uleth.ca (R.J. McDonald), mohajerani@uleth.ca (M.H. Mohajerani).

0197-4580/$ – see front matter © 2018 Elsevier Inc. All rights reserved.
https://doi.org/10.1016/j.neurobiolaging.2018.10.026

Bea et al., 2005). Although there is some controversy surrounding the issue of cholinergic neuronal death, there is no doubt that cholinergic tone is altered in patients with AD (Craig et al., 2011; Francis et al., 1999; Frölich et al., 2002). Moreover, the increased activity of acetyl cholinesterase causes hydrolysis of acetylcholine and has also been reported within and around Aβ plaque in transgenic mouse models of AD (Sberna et al., 1998).

Several experimental models such as chimpanzees, tree shrews, beagles, mice, rats, rabbits, zebrafish, fruit flies, ascidians, and yeasts are being used to study the pathological and behavioral aspects of AD (Li, 2013; Li et al., 2016). Of these models, mouse models are used commonly to study the pathology and to investigate drug treatments for AD (Cavanaugh et al., 2014; Hall and Roberson, 2012). In last two decades, more than 400 drugs failed in clinical trials, which may be due to various factors such as inappropriate choice of mouse models, wrong timing for therapeutic interventions, over-reliance on inappropriate assays for translational studies, or lack of precise biomarkers (Sasaguri et al., 2017). In a review, Sasaguri et al. also discussed the suitable application and limitations of currently available amyloid precursor protein (APP) mouse models for AD (Sasaguri et al., 2017). Available transgenic mouse models of AD show an overexpression of APP and APP fragments; as a result, mice suffer from artificial phenotypes (Hsiao et al., 1996; Saito et al., 2014). Saito et al. developed a single APP knock-in (APP-KI) mouse model for AD to overcome problems with APP overexpression (Saito et al., 2014). In addition, overproduction of APP, C-terminal fragment (βCTF-β/α), and APP intracellular domain were observed in APP-transgenic mice (APP23) when compared to $APP^{wt/wt}$ and $APP^{NL\text{-}F/NL\text{-}F}$ mice (Saito et al., 2014). $APP^{NL\text{-}F/NL\text{-}F}$ mice also produced more Aβ42 with the highest Aβ42/Aβ40 ratio than any other mouse model. Furthermore, $APP^{NL\text{-}G\text{-}F/NL\text{-}G\text{-}F}$ mice showed APP expression and processing identical to that of $APP^{NL\text{-}F/NL\text{-}F}$ mice (Saito et al., 2014). Saito et al also reported that these mice showed the Aβ pathology, synaptic dysfunction, and neuroinflammation (Saito et al., 2014). The $APP^{NL\text{-}G\text{-}F/NL\text{-}F\text{-}F}$ mouse showed memory impairment in Y-maze at the age of 6 months. Moreover, in a previous study, enhanced compulsive behavior and reduced attention performance of APP-KI mice has been reported (Masuda et al., 2016). In addition, changes in social, anxiety-related test performance and open-field activity behavior were reported in previous studies (Hernandez et al., 2017; Whyte et al., 2018). However, these studies lack a detailed behavioral and pathological characterization of this mouse model in an age-dependent manner. In addition, researchers have not investigated the amyloid plaque distribution in different brain regions such as the medial septum-diagonal band (MSDB) complex, caudate-putamen (CPu), cerebellum, hindbrain, and locus coeruleus (LC) as these brain regions are also associated with various cognitive functions including learning and memory.

The present study was designed to perform behavioral and pathological characterization of $APP^{NL\text{-}G\text{-}F/NL\text{-}G\text{-}F}$ mice, a novel mouse model of AD, in age-dependent manner. Various behavioral paradigms designed to assess different types of learning and memory functions such as Morris water maze (MWM), object recognition test, fear conditioning (FC) test and the general activity test at the age of 3, 6, 9, and 12 months were performed. At the study endpoint, immunostaining for amyloid plaques, ChAT, a cholinergic marker, tyrosine hydroxylase (TH), a rate-limiting enzyme in norepinephrine (NE) synthesis pathway and glial fibrillary acidic protein (GFAP) were performed.

2. Materials and methods

2.1. Animals and experimental design

The male and female pairs of APP-KI mice carrying Arctic, Swedish, and Beyreuther/Iberian mutations ($APP^{NL\text{-}G\text{-}F/NL\text{-}G\text{-}F}$) were gifted by RIKEN Center for Brain Science, Japan. The colony of these mice was maintained in our animal house at Canadian Center for Behavioral Neuroscience. Genotyping of all mice was done by polymerase chain reaction using ear-notching method. C57BL/6J mice were used as a control. Animals were group-housed 4 mice in each cage in a controlled environment (22 °C–25 °C, 50% humidity and a 12-hour light:dark cycle) with free access to standard laboratory chow and water. All experimental procedures were approved by the institutional animal care committee and performed in accordance with the standards set out by the Canadian Council for Animal Care. In the present study, we used 40 male C57BL/6J and 40 male $APP^{NL\text{-}G\text{-}F}$ mice for our experiment. We performed behavioral tests and biochemical assays in mouse's brain when they were 3, 6, 9, and 12 months old. We used 10 mice for behavioral tests and 4 mice for immunohistochemistry at each of the testing age points. We used separate cohort of mice at each test point to avoid the recurrent exposure to various behavioral tasks. The samples size in the present study for behavioral parameters and for immunostaining was calculated based on our pilot experiments, and during the sample size calculation we considered alpha = 0.05, power > 80%. Post hoc power analyses indicated that power was sufficient enough to detect any existing effects. In the present study, we did not use the female mice as no difference in amyloid pathology and inflammatory responses in male and female $APP^{NL\text{-}G\text{-}F}$ mice has already been reported in previous studies (Masuda et al., 2016; Peters et al., 2018). Masuda et al. also mentioned that effect of pathologic Aβ accumulations on behavior has low sensitivity to sex-dependent factors (Masuda et al., 2016).

2.2. Behavioral study

Various behavioral paradigms (MWM, novel object recognition, FC test, and general activity cage test) were performed for 3-, 6-, 9-, and 12-month-old mice. FC test was done at the end of all behavioral tests to rule out shock-induced fear as a confounding factor. The behavioral assessment performed by the researcher at each of the testing points was blinded to the experimental groups.

2.2.1. Morris water maze

All water maze experiments were performed in a circular tank (154 cm in diameter, 50 cm deep) with slight modification (Kee et al., 2007; Mehla et al., 2018a). The tank was filled to a depth of 40 cm with water and made opaque by adding nontoxic white tempera paint. Water temperature was maintained at 22 ± 1 °C to prevent the mouse from floating. A circular escape platform (11 cm radius) was placed 0.5–1 cm below the water surface in one of four quadrants. Three distinct cues of different geometry were used around the tank to help the mouse navigate to the platform position. Mice were individually handled each day for 1 week before starting the acquisition training. In the MWM maze, mice are slow learners, so mice require more days of training in the MWM. Therefore, 8 days of acquisition trials was given. On each acquisition day, mice received 4 training trials from each quadrant in distributed manner for 8 days. The trial was completed once the mouse found the platform or 60 seconds had elapsed. If the mouse failed to find the platform on a given trial, the mouse was guided onto the platform. The latency to reach the platform was analyzed to confirm the learning behavior of the mice. The swim speed was analyzed to rule out the involvement of motor function as a confounding factor. A single probe trial was conducted on day 9 to assess the integrity and strength of spatial memory 24 hours after the completion of the last trial of the acquisition phase. The data in the probe trial were analyzed measuring the time spent by mice in the target quadrant and average proximity to the escape annulus.

We also performed a visible platform test of the MWM as described previously (Mehla et al., 2018a) to rule out the involvement of potential sensory, motor, and motivation impairments as noncognitive confounding factors during spatial navigation in the mutant mice. In this test, the platform was made visible by keeping the platform 1–2 cm above the water level and marked with a black tape so that mice could see the platform. The cued-platform task was carried out for 2 days after performing the probe test and consisted of one training session each day. Each session contained 8 trials (lasting 60 seconds). The platform was placed at different locations during the sessions 1 and 2. The latency to reach the platform in each session was noted as an indicator of mice learning ability.

2.2.2. Novel object recognition test

The novel object recognition test was conducted as described previously (Vogel-Ciernia and Wood, 2014). This test is based on the principle that mice will explore novel items. When mice are made familiar with two similar objects during the training day, they will spend more time exploring a novel object on a subsequent test day, when in a familiar environment (Antunes and Biala, 2012). Briefly, mice were brought from their home cage to the experimental room and habituated to testing box for 5 minutes daily for 6 days. 24 hours after the last habituation day, training was performed. Two familiar objects were cleaned with 70% isopropyl alcohol to mask any previous order cues and allowed to dry completely. The familiar objects were placed in the testing box at equal distances from the walls. A video camera was setup to record the mice's behavior for further analysis. The mice were introduced into the testing box for 10 minutes to explore both familiar objects, and recordings were made for each mouse. The test session was performed 24 hours after training. In the test session, one of the familiar objects was replaced with a novel object with different geometry and texture. These objects were cleaned with 70% isopropyl alcohol and allowed to dry completely. Mice were individually placed in the testing box for 5 minutes to explore the objects, and a recording of their behavior was made for each mouse. After each mouse completed the test, feces were removed and bedding was stirred to equally distribute any odor cues. The objects were also wiped with 70% isopropyl alcohol to mask the odor cues after each mouse. The data were analyzed by measuring the exploration time for familiar and novel object during training and testing days. The investigation ratio was calculated for each group.

2.2.3. Fear conditioning test

FC was conducted as described previously with slight modifications (Wiltgen et al., 2005; Zuloaga et al., 2016). This test is used to assess the amygdala- and hippocampus-dependent memory in rodents. FC was conducted in an acrylic square box (33 × 33 × 25 cm). A video camera was fixed to record the mice's behavior for further analysis. The floor of chamber consisted of 64 stainless steel rods (2 mm diameter) spaced 5 mm apart. The rods were connected to a shock generator for the delivery of a footshock. A speaker was used to deliver the tone stimulus. Before conditioning, the chamber was cleaned with a 1% Virkon solution to mask any previous odor cues. The tone test was conducted in a triangular chamber (33 × 33 × 29 cm) that was structurally different than the conditioning chamber. Before starting the tone test, the chamber was cleaned with a 70% isopropyl solution. On the conditioning day, mice were brought from their home cage into a testing room and allowed to sit undisturbed in their cages for 10 minutes. Mice were then placed in the conditioning square box and allowed to explore for 2 minutes before the onset of the tone (20 seconds, 2000 Hz). In the delay conditioning procedure, a shock (2 seconds, 0.5 mA) was given in the last 2 seconds of tone duration. The mice received five delayed conditioning trials, each separated by a 120-second intertrial interval. The mice were taken from the conditioning chambers 1 minute after the last shock and returned to their home cages. 24 hours later, the mice were placed in a triangular box to assess conditioning to the tone in the absence of the training context. For the tone test, three 20-second tones were given after a 2-minute baseline period. Each tone presentation was separated by a 120-second intertrial interval. The freezing response was measured using a time sampling procedure in which an observer scored the presence or absence of the freezing response for each mouse at every 2-second interval. 24 hours after the tone test, mice were placed back in the original conditioning box for a 5-minute context test. During this test, freezing was scored for each mouse at every 5-second interval. Data were transformed into a percent freezing score by dividing the number of freezing observations by the total number of observations and multiplying by 100. During the conditioning and context procedures, the box was cleaned with 1% Virkon; the tone procedure box was cleaned with 70% isopropyl after each mouse trial to mask any odor cues left by the previous subject and discern context.

2.2.4. Novelty-associated general locomotor activity

The novelty-induced behavior was evaluated using an automated open-field test (VersaMax Animal Activity Monitoring System, AccuScan Instrument Inc, USA) as described in the instrument manual. The open-field activity monitoring system is used to assess the locomotive function of rodents. The test is also widely used to assess anxiety-like and exploratory behaviors. This system consisted of 6 animal monitoring chambers (16 in × 16 in × 12 in) covered by transparent lids with perforations, an analyzer and a computer. The base of each monitoring chamber was lined with vertical and horizontal laser generators and sensors. The behaviors of interest were predefined into the system. During the test, any behavior exhibited by the animals in the monitoring chamber was transmitted to the analyzer, recorded on a computer, and the data subsequently exported to Microsoft Excel. The animals were placed individually into the open-field observational box and recorded for 10 minutes. Novelty-associated general locomotor activity was assessed by measuring horizontal activity, vertical activity, total distance traveled, total move number, total move time, margin, and center distance traveled. Novelty-induced rearing was counted as the number of times the mouse stood on its hind limbs with its forelimbs against the wall of the observation cage (supported rearing) or in free air (unsupported rearing). The number of rearing (both supported and unsupported) was recoded for 10 minutes.

2.3. Immunohistochemistry

Mice were transcardially perfused with phosphate-buffered saline (PBS) and 4% paraformaldehyde in PBS. Brains were collected for immunohistochemical analysis. The brains were kept in 4% paraformaldehyde for 24 hours and transferred to 30% sucrose after rinsed with PBS. Brains were stored at 4 °C until sectioning. Brains were serially sectioned coronally at 40 μm on a freezing microtome. Immunohistochemical procedures for 4G8, GFAP, ChAT, and TH were performed as previously described, with slight modifications (Masuda et al., 2016; Mehla et al., 2018b; Saito et al., 2014). In brief, sections were fixed on positively subbed slides. For 4G8 immunostaining, antigen retrieval was performed by incubating the sections for 10–15 minutes in 70% formic acid. Slides were washed in Tris-buffered Saline (TBS), permeabilized with 0.1% Triton-X in TBS, and then blocked in a solution containing 2% bovine serum albumin and 0.1% Triton-X in TBS. The sections were incubated for 48 hours in primary antibody at room temperature in a dark humid chamber.

For all other labeling, after TBS washes, slides were blocked for 2 h in TBS containing 0.3% Triton-X and 3% goat serum. Primary antibodies were added in TBS with 0.3% Triton-X for 24h at room temperature in a humid chamber.

The following primary antibodies were used: mouse anti-amyloid-β 4G8 (BioLegend, 1:1000); rabbit anti-GFAP (Ab7260, Abcam, 1:2000); mouse anti-NeuN primary antibody (monoclonal, Millipore, MAB377, 1:1000); rabbit anti-ChAT (monoclonal, Abcam, ab178850, 1:5000), and rabbit anti-Tyrosine-hydroxylase (Ab112, Abcam, 1:3000). Following incubation, three 10-minute washes were given, and sections were incubated with secondary antibody for 24 hours. The following secondary antibodies were used: goat anti-mouse-alexa-488 (IgG [H + L], ab150113, Abcam, 1:1000) and goat anti-rabbit-alexa-594 (IgG [H + L], A11037, Invitrogen, 1:2000 for GFAP, 1:3000 for ChAT, 1:5000 for TH). The sections were mounted on microscope slides, dehydrated, and covered with coverslips with Vectashield H-1000 (Vector Laboratory). Finally, whole slides were imaged using NanoZoomer microscope (NanoZoomer 2.0-RS, HAMAMATSU, JAPAN). We analyzed 3 brain sections for immunostaining markers for each mouse, and analysis was conducted by a researcher who was blinded to which experimental group the brain belonged. The images were analyzed using ImageJ software.

2.4. Statistical analysis

The statistical analysis was performed using SPSS statistical software package, version 22.0. Results are presented as mean ± SEM. One-way analysis of variance with repeated measures was used to find statistically significant differences across the days during the acquisition phase. Paired *t*-test was used to measure any significant differences during the probe trial. The statistically significant differences between the groups were evaluated using independent Student's t-test. A p value <0.05 was considered as statistically significant.

3. Results

3.1. Assessment of age-dependent learning and memory functions of APP^{NL-G-F} mice using Morris water maze

3.1.1. Acquisition phase

Three-month-old C57BL/6J and APP^{NL-G-F} mice showed a standard learning curve in the MWM evidenced by a significant ($F_{(7,63)}$ = 12.756, p = 0.000 for C57BL/6J and $F_{(7,63)}$= 14.749, p = 0.000 for APP^{NL-G-F}) decrease in latency on day 8 (13.97 ± 1.55 seconds for C57BL/6J and 12.24 ± 1.54 seconds for APP^{NL-G-F}) in comparison to day 1 (45.57 ± 3.0 seconds for C57BL/6J and 46.32 ± 4.34 seconds for APP^{NL-G-F}, Fig. 1A). No significant difference for trial latency was found on day 8 between C57BL/6J and APP^{NL-G-F} mice (Fig. 1A). The swim speed of C57BL/6J and APP^{NL-G-F} mice did not change significantly during acquisition, indicating normal motor performance of the mice (Fig. 1E). At the age of 6 months, both C57BL/6J and APP^{NL-G-F} mice learned the task, evidenced by a significant ($F_{(7,63)}$ = 17.418, p = 0.000 for C57BL/6J and $F_{(7,63)}$ = 3.146, p = 0.006 for APP^{NL-G-F}) decrease in latency from day 1 to day 8 (Fig. 1B). Independent *t*-test analysis showed a significant

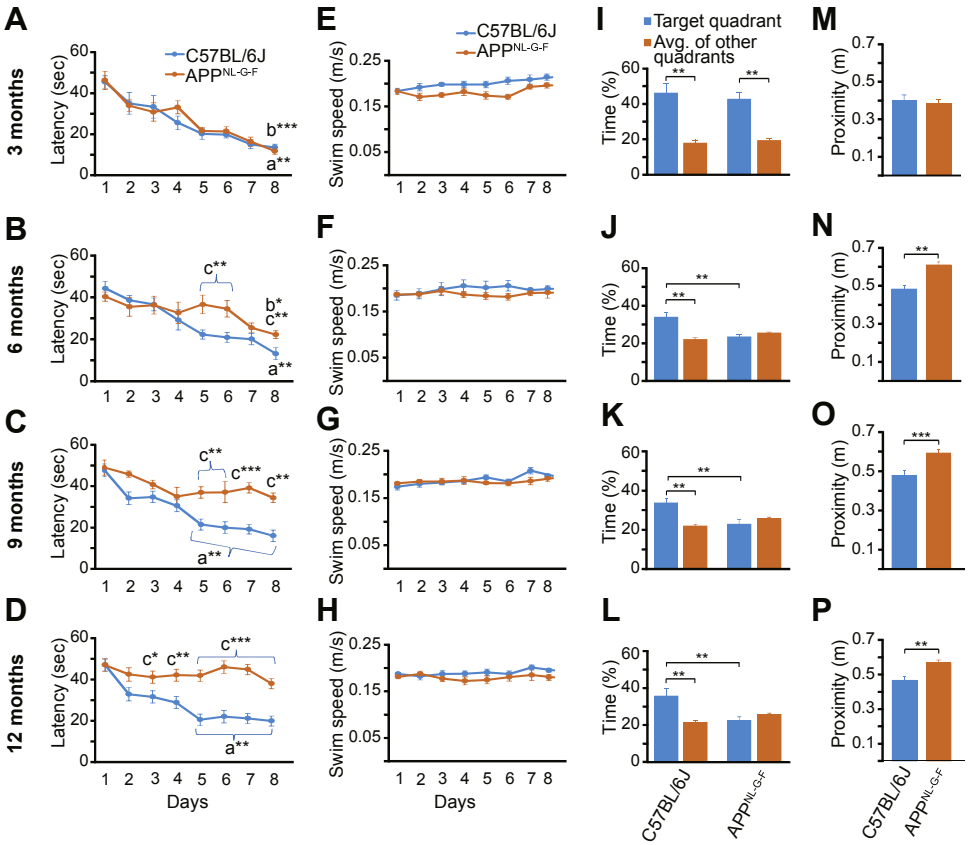

Fig. 1. Evaluation of spatial learning and memory performance of APP^{NL-G-F} mice in the Morris water maze via analyzing (A-D) latency during the acquisition phase indicating the learning power of mice; (E-H) swim speed during the acquisition phase; (I-L) percent time spent by mice in target quadrant and average of other quadrants during the probe trial; (M-P) average proximity to the platform during the probe trial. Supplementary Fig. 1 represents age-dependent comparison of spatial learning and memory functions of C57BL/6J mice (A–D) and APP^{NL-G-F} mice (E–H). The results were expressed as mean ± SEM. *$p < 0.05$; **$p < 0.01$; ***$p < 0.001$; a-as compared with day 1 for C57BL/6J mice; b-as compared with day 1 for APP^{NL-G-F}; c-as compared with C57BL/6J mice; (n= 10 for C57BL/6J mice; n= 10 for APP^{NL-G-F} mice).

($t_{(18)}$= −4.106, $p = 0.001$) difference in the latency on day 8 between C57BL/6J and APP^{NL-G-F} group indicating impaired learning ability of APP^{NL-G-F} mice (Fig. 1B). No significant difference was found in the swim speed of C57BL/6J and APP^{NL-G-F} mice across the acquisition days (Fig. 1F). A normal learning curve for 9-month-old C57BL/6J mice was observed in MWM test, indicated by significant ($F_{(7,63)}$= 15.480, $p = 0.000$) decrease in latency to find hidden platform on day 8 as compared with day 1 (Fig. 1C). However, 9-month-old APP^{NL-G-F} mice showed an impaired learning curve indicated by no significant difference in the latency between days 1 (48.99 ± 3.64 seconds) and 8 (34.37 ± 4.67 seconds) (Fig. 1C). Independent *t*-test analysis showed a significant ($t_{(18)} = -3.413$, $p = 0.003$) difference in the latency to reach the platform on day 8 between C57BL/6J and APP^{NL-G-F} mice indicating an impaired learning ability of APP^{NL-G-F} mice (Fig. 1C). The motor performance appeared normal which is evidenced by a nonsignificant difference in mice swim speed across the acquisition days (Fig. 1G). The swim speed of C57BL/6J mice was not statistically different from APP^{NL-G-F} mice (Fig. 1G). Twelve-month-old C57BL/6J mice showed a very clear learning curve in this task, indicated by a significant ($F_{(7,63)}$ = 10.745, $p = 0.000$) decrease in latency to reach the platform on day 8 when compared with day 1 (Fig. 1D). The learning ability of APP^{NL-G-F} mice was completely impaired at 12 months of age, which is supported by a nonsignificant ($F_{(7,63)} = 1.311$, $p = 0.260$) decrease in latency from day 1 to day 8 (Fig. 1D). At 12 months of age, a nonsignificant difference was found in the swim speed of C57BL/6J and APP^{NL-G-F} mice across the training days (Fig. 1H). The swim speed of APP^{NL-G-F} mice was not statistically different from C57BL/6J mice (Fig. 1H). An age-dependent analysis was performed for C57BL/6J and APP^{NL-G-F} mice using one-way analysis of variance with Bonferroni post hoc test. No significant difference in the learning curves for C57BL/6J across the age was found, as indicated by a nonsignificant ($F_{(3)}$= 1.336, $p = 0.278$) difference in the latency on day 8 at the age of 3, 6, 9, and 12 months (Supplementary Fig. 1A). APP^{NL-G-F} mice showed an age-dependent impairment in the learning ability indicated by a significant ($F_{(3)} = 25.254$, p = 0.000) increase in the latency to reach platform on day 8 at the age of 6, 9, and 12 months in comparison to 3 months (Supplementary Fig. 1E). The swim speed of C57BL/6J and APP^{NL-G-F} mice did not change significantly across the ages (Supplementary Fig. 1B and F, respectively).

3.1.2. Probe trial

The results from the probe trial showed a spatial memory retention in both C57BL/6J and APP^{NL-G-F} mice at the age of 3 months (Fig. 1I). The percent time spent in the target quadrant by C57BL/6J and APP^{NL-G-F} mice was significantly ($t_{(9)} = 4.059$, p = 0.003 for C57BL/6J and $t_{(9)} = 4.773$, $p = 0.001$) higher in comparison to the average percent time spent in other quadrants; this suggests that the animals exhibited a less diffuse search pattern, with a spatial bias toward the former training quadrant (Fig. 1I). No significant difference in the time spent by mice in target quadrant and average proximity from platform between the C57BL/6J and APP^{NL-G-F} groups was found (Fig. 1I and M). At the age of 6 months, C57BL/6J mice spent significantly ($t_{(9)} = 3.125$, $p = 0.012$) more time in the target quadrant compared with other quadrants, suggesting spatial memory retention (Fig. 1J). No significant ($t_{(9)} = -1.176$, p = 0.270) difference was found in time spent by APP^{NL-G-F} mice in the target quadrant compared with other quadrants (Fig. 1J). APP^{NL-G-F} mice spent significantly ($t_{(18)} = 3.325$, $p = 0.004$) less time in target quadrant when compared with C57BL/6J mice (Fig. 1J). The average proximity from the platform was significantly ($t_{(18)} = -5.465$, p = 0.000) higher in the APP^{NL-G-F} group as compared with C57BL/6J group suggesting that the APP^{NL-G-F} mice retained a less accurate spatial memory (Fig. 1N). Results from the probe trial indicate an impairment of spatial memory function of APP^{NL-G-F} mice at the age of 6 months. At the age of 9 and 12 months, C57BL/6J did not show impairment of memory function (Fig. 1K and L, respectively). Spatial memory impairment was observed in APP^{NL-G-F} mice when they were 9 and 12 months old, which is evidenced by no significant difference between the time spent by APP^{NL-G-F} mice in target quadrant and other quadrants (Fig. 1K and L, respectively). When compared with C57BL/6J, APP^{NL-G-F} mice spent significantly ($t_{(18)}$ = 3.407, p = 0.003 for 9 months; $t_{(18)}$ = 3.055, p = 0.001 for 12 months) less time in target quadrant indicating impaired memory function of APP^{NL-G-F} mice (Fig. 1K and L, respectively). A significantly higher average proximity for APP^{NL-G-F} mice in comparison with C57BL/6J mice at the age of 9 and 12 months was found, showing a diffuse swim path pattern (Fig. 1O and P, respectively).

In an age-dependent analysis, C57BL/6J did not show memory impairment at the age of 6, 9, and 12 months when compared with 3 months, evidenced by latency to reach the platform on day 8 during training phase and the amount of time spent in the target quadrant and average proximity to the platform in the probe trial (Supplementary Fig. 1C and D). Memory impairment was found in APP^{NL-G-F} mice at the age of 6, 9, and 12 months in comparison to 3 months as shown by latency to reach the platform on day 8 during the learning phase and time spent in the target quadrant and average proximity to the platform during the probe test (Supplementary Fig. 1G and H).

3.1.3. Visible platform test

C57BL/6J and APP^{NL-G-F} mice were tested in the cued version of the MWM test, which does not require spatial learning and memory functions. The cued version of the MWM test was used to rule out the possibility of the impact of noncognitive factors on spatial navigation. The latency to reach the visible platform for C57BL/6J and APP^{NL-G-F} mice was decreased significantly from session 1 to session 2 at all test age points (Supplementary Fig. 2A–D). No statistically significant difference was found in latency between C57BL/6J and APP^{NL-G-F} mice (Supplementary Fig. 2A–D). These results indicate that the impairment in spatial memory found in APP^{NL-G-F} mice was not due to impairments in visual acuity, sensorimotor functions, or motivation.

3.2. Assessment of age-dependent aversive associative learning and memory of APP^{NL-G-F} mice using a fear conditioning test

No significant difference was found between the percent freezing for C57BL/6J and APP^{NL-G-F} mice at the age of 3 months (Fig. 2A) in a cued FC test. At the age of 6 months, APP^{NL-G-F} mice showed a significantly (81.67 ± 1.24% for C57BL/6J and 48.33 ± 1.94% for APP^{NL-G-F}; $t_{(18)} = 14.467$, $t = 0.000$) lower percent freezing time in comparison with C57BL/6J mice (Fig. 2B). APP^{NL-G-F} mice showed a significantly (84.67 ± 1.87% for C57BL/6J and 52.67 ± 2.42% for APP^{NL-G-F}; $t_{(18)}$ = 10.447, p = 0.000) lower percent freezing in comparison to C57BL/6J at 9 months (Fig. 2C). A significantly (87.32 ± 3.87% for C57BL/6J and 50.67 ± 4.15% for APP^{NL-G-F}; $t_{(18)} = 6.457$, $p = 0.000$) lower percent freezing time was found in APP^{NL-G-F} mice when compared to C57BL/6J mice at the age of 12 months (Fig. 2D). In addition, in contextual FC test, the APP^{NL-G-F} mice showed age-dependent memory impairment (Fig. 2B–D). These results indicate that APP^{NL-G-F} mice showed evidence of a tone-shock and contextual associative memory impairment at the age of 6, 9, and 12 months. During the baseline recording, the first 2 minutes of the cued FC test, no significant change in freezing behavior across the testing points was found (data not shown) indicating normal locomotor activity. An age-dependent analysis of C57BL/6J mice showed no significant difference in the percent

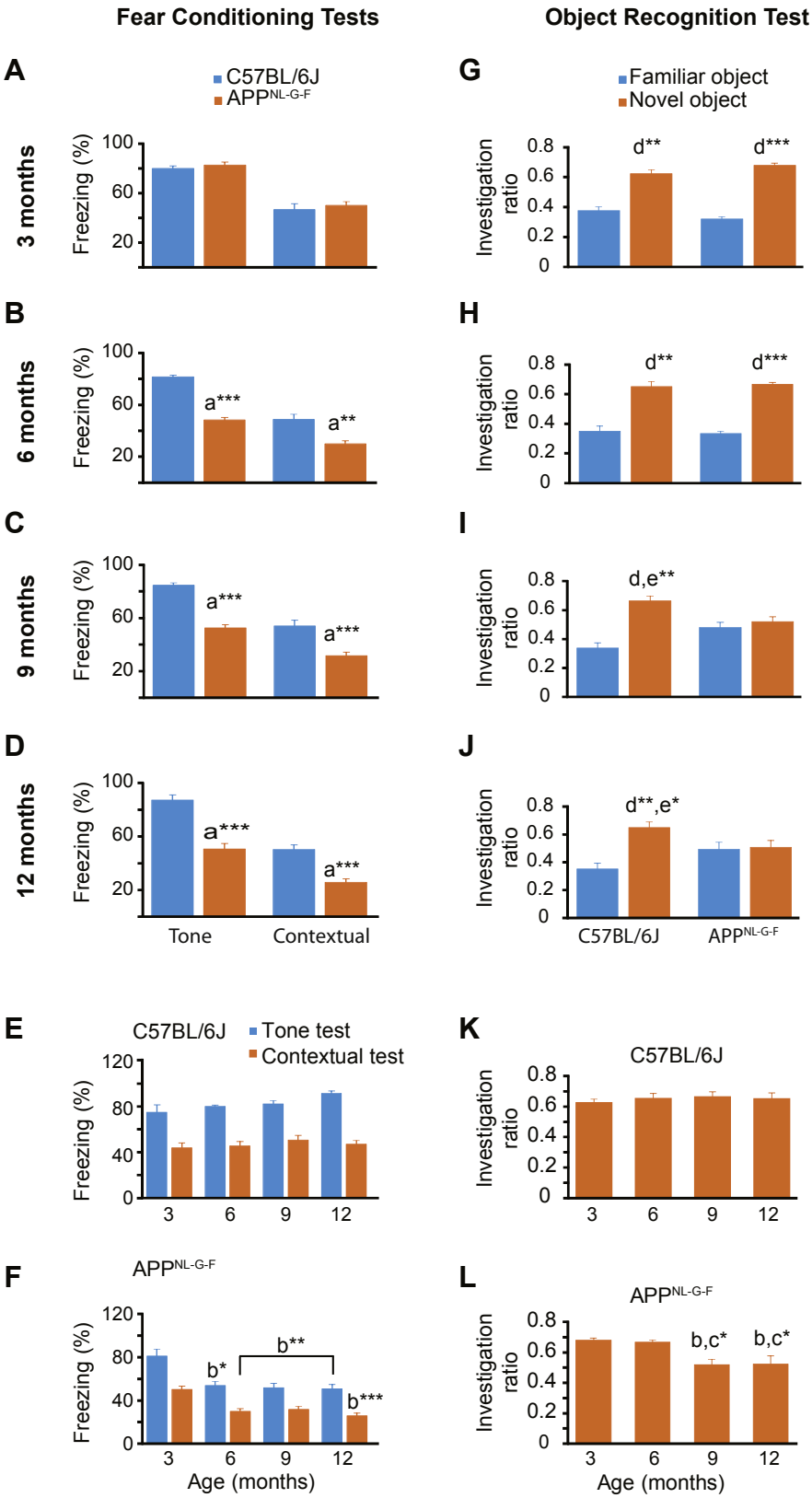

Fig. 2. APP^{NL-G-F} mice were impaired in fear conditioning and novel object recognition tests. (A-D) Percent freezing of mice during tone and contextual fear conditioning test. (E) Age-dependent comparison of percentage of freezing of C57BL/6J mice during tone and contextual fear conditioning tests. (F) Age-dependent comparison of percentage of freezing of APP^{NL-G-F} mice during tone and contextual fear conditioning tests. (G-J) investigation ratio for C57BL/6J and APP^{NL-G-F} mice in object recognition test. (K) Age-dependent comparison of investigation ratio of C57BL/6J mice in the object recognition test. (L) Age-dependent comparison of investigation ratio of APP^{NL-G-F} mice in the object recognition test. The results were expressed as mean ± SEM. $^{*}p < 0.05$, $^{**}p < 0.01$, $^{***}p < 0.001$; a-as compared with C57BL/6J mice; b-as compared with 3-month-old APP^{NL-G-F} mice; c-as compared with 6-month-old APP^{NL-G-F} mice; d-as compared with familiar object; e-as compared with novel object (n = 10 for C57BL/6J mice; n = 10 for APP^{NL-G-F} mice).

freezing time to the trained tone and contextual as a function of age (Fig. 2E). APP^{NL-G-F} mice showed significantly reduced percent freezing time to the trained tone and context at the age of 6, 9, and 12 months in comparison to 3 months (Fig. 2F).

3.3. Assessment of age-dependent object recognition memory functions of APP^{NL-G-F} mice using object recognition test

Both C57BL/6J and APP^{NL-G-F} mice showed normal memory function at 3 and 6 months of age, indicated by a significant difference between investigation ratios for novel and familiar objects (Fig. 2G and H, respectively). No significant difference in investigation ratios between C57BL/6J and APP^{NL-G-F} mice at the age of 3 and 6 months was found (Fig. 2G and H, respectively). At the age of 9 and 12 months, C57BL/6J mice performed normally as shown by a significantly higher investigation ratio for the novel object compared to the familiar object, indicating that these mice are spending more time exploring the novel object, indicating normal recognition memory function (Fig. 2I and J, respectively). No significant difference was found between investigation ratio for novel and familiar object at the age of 9 ($t_{(9)} = -0.570$, $p = 0.583$) and 12 ($t_{(9)} = -0.135$, $p = 0.896$) months for the APP^{NL-G-F} mice, indicating impairment of associative memory of these mice (Fig. 2I and J, respectively). In comparison to C57BL/6J, APP^{NL-G-F} mice showed significantly reduced investigation ratio for novel object at the age of 9 ($t_{(18)} = 2.911$, $p = 0.009$) and 12 ($t_{(18)} = 2.185$, $p = 0.042$) months, showing memory impairment in these mice (Fig. 2I and J, respectively).

An age-dependent analysis showed no significant change in the investigation ratio of C57BL/6J mice across the ages (Fig. 2K). APP^{NL-G-F} mice showed memory impairment at the age of 9 and 12 months in comparison to 3 and 6 months indicated by significantly less time spent by mice exploring the novel object (Fig. 2L).

3.4. Assessment of age-dependent novelty-induced general activity of APP^{NL-G-F} mice

Spontaneous locomotor activity of mice was assessed by measuring the horizontal activity, vertical activity, total distance traveled, total move number, and total move time. The rearing activity of mice indicates exploratory behavior, and anxiety-related behavior was assessed by measuring the margin and center distance traveled by mice. No significant difference was observed in the horizontal activity, vertical activity, total distance traveled, total move number, total move time, margin and center distance traveled, and rearing activity between C57BL/6J and APP^{NL-G-F} mice at 3, 6, 9, and 12 months (Table 1). No significant difference was found in the horizontal activity, vertical activity, total distance traveled, total move number, total move time, and center distance traveled and rearing activity of C57BL/6J mice across the age (Table 1). APP^{NL-G-F} mice did not show any significant change in these different measures of general activity across the various test points (Table 1).

3.5. Amyloid pathology, astrocytosis, cholinergic and noradrenergic dysfunction

In APP^{NL-G-F} mice, the amyloid plaque burden was increased with age (Fig. 3A and D). A significant increase in the amyloid deposition was observed at the age of 6, 9, and 12 months of APP^{NL-G-F} mice in the cortex (Fig. 3D) and hippocampus (Fig. 3E) when compared to 3-month-old APP^{NL-G-F} mice. In addition, a significant increase in amyloid load was also found in LC of 9- and 12-month-old APP^{NL-G-F} mice (Fig. 5A and C). Supplementary figures showed a significant increase in the amyloid deposition in MSDB complex (Fig. S4A and B), CPu (Fig. S4C and D), hindbrain (Fig. S5A and B), and cerebellum (Fig. S5C and D) of 6-, 9-, and 12-month-old APP^{NL-G-F} mice in comparison with 3-month-old APP^{NL-G-F} mice. In the cortex (Fig. 3D), hippocampus (Fig. 3E), MSDB complex (Supplementary Fig. 4B), and hindbrain (Supplementary Fig. 5B), no significant difference was found in 9- and 12-month-old APP^{NL-G-F} mice, indicating amyloid deposition peaks around 9 months. We also found significant increases in amyloid plaque load in CPu (Supplementary Fig. 4D), cerebellum layers (Supplementary Fig. 5D), and LC (Fig. 5C) of 12-month-old APP^{NL-G-F} mice when compared with 9-month-old mice.

Age-dependent increase in astrocytosis was found in the cortex at 6-, 9-, and 12-month-old APP^{NL-G-F} mice in comparison with C57BL/6J and 3-month-old APP^{NL-G-F} mice (Fig. 3F). However, 9- and 12-month-old APP^{NL-G-F} mice showed a significant increase in GFAP expression in the hippocampus when compared with C57BL/6J and 3- and 6-month-old APP^{NL-G-F} mice (Fig. 3G). An increase in astrocytosis was observed in the MSDB complex (Supplementary Fig. 4F), CPu (Supplementary Fig. 4H), hindbrain (Supplementary Fig. 5F), and cerebellum layers (Supplementary Fig. 5H) of APP^{NL-G-F} mice in comparison with C57BL/6J mice. No significant difference was found in astrocytosis in the cortex (Fig. 3F), hippocampus (Fig. 3G), MSDB complex (Supplementary Fig. 4F), hindbrain (Supplementary Fig. 5F), and cerebellum layers (Supplementary Fig. 5H) of 9- and 12-month-old APP^{NL-G-F} mice. However, 12-month-old APP^{NL-G-F} mice showed significantly more astrocytosis in comparison with 9-month-old APP^{NL-G-F} mice. The astrocytosis was at maximum when the APP^{NL-G-F} mice were 9 and 12 months old.

In term of cholinergic function, we found a significant decrease in ChAT-positive neurons in the MSDB complex of 6-, 9-, and 12-month-old APP^{NL-G-F} mice in comparison to C57BL/6J and

Table 1
Assessment of age-dependent novelty-associated general activity of C57BL/6J and APP^{NL-G-F} mice

General activity measurement	Groups							
	C57BL/6J				APP^{NL-G-F}			
	Age (months)				Age (months)			
	3	6	9	12	3	6	9	12
Horizontal activity	3522.3 ± 233.6	3362.9 ± 264.6	3630.7 ± 276.6	3725.8 ± 273.5	3091.0 ± 212.9	3445.4 ± 213.2	3205.2 ± 284.9	3078.3 ± 258.1
Total distance (cm)	1482.0 ± 125.3	1486.5 ± 190.5	1701.1 ± 135.4	1617.3 ± 160.8	1578.6 ± 130.6	1577.0 ± 155.3	1664.6 ± 76.5	1769.8 ± 120.1
Move number	149.2 ± 6.9	134.8 ± 9.9	141.8 ± 5.2	148.2 ± 4.8	134.6 ± 7.8	134.4 ± 7.3	127.9 ± 9.6	140.6 ± 3.9
Move time (sec)	149.5 ± 12.5	131.1 ± 13.3	159.8 ± 15.4	152.8 ± 15.6	143.9 ± 11.8	144.2 ± 13.1	140.3 ± 11.3	160.3 ± 9.4
Vertical activity	200.4 ± 17.2	179.6 ± 27.6	225.6 ± 17.0	221.3 ± 10.7	183.6 ± 23.3	189.6 ± 18.9	208.3 ± 10.4	207.5 ± 11.5
Margin distance (cm)	1039.0 ± 121.4	1006.9 ± 94.9	1143.4 ± 55.9	1019.3 ± 67.7	1087.8 ± 71.4	1104.2 ± 102.7	1014.0 ± 158.7	1241.9 ± 81.1
Center distance (cm)	544.2 ± 69.8	481.0 ± 113.9	557.9 ± 93.9	599.1 ± 97.5	591.3 ± 66.5	472.6 ± 54.9	518.3 ± 46.9	527.6 ± 43.9
Rearing activity	198.2 ± 16.7	174.8 ± 26.2	221.9 ± 16.5	219.3 ± 10.7	181.3 ± 23.0	183.0 ± 18.1	200.9 ± 13.1	205.6 ± 11.4

Data are presented as mean ± SEM.

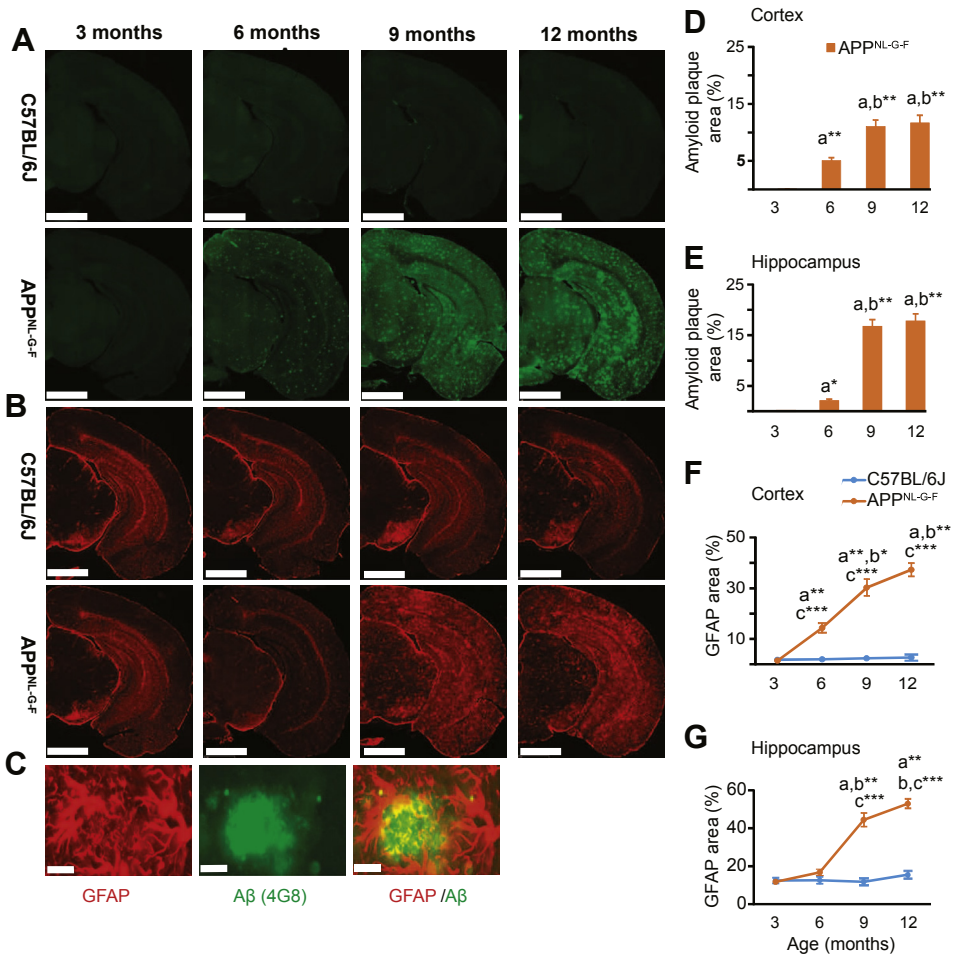

Fig. 3. Amyloid plaque distribution and astrocytosis in different brain regions of APP^{NL-G-F} mice (n= 4) at the age of 3, 6, 9, and 12 months. (A) Photomicrographs of immunohistochemistry staining of 4G8 (green, antibody is reactive to amino acid residues 17-24 of amyloid-β) in the cortex and hippocampus. (B) Photomicrographs of immunohistochemistry staining of GFAP (red, indicator of astrocytosis) in the cortex and hippocampus. (C) Representation of astrocytosis around the amyloid plaque area. (D) Representation of percent amyloid plaque area in the cortex at the age of 3, 6, 9, and 12 months; (E) representation of percent amyloid plaque area in the hippocampus at the age of 3, 6, 9, and 12 months; (F) representation of percent astrocytosis in the cortex at the age of 3, 6, 9, and 12 months; (G) representation of percent astrocytosis in the hippocampus at the age of 3, 6, 9, and 12 months. Scale bars represent 2.5 mm for panel A and B and 25 μm for panel C. Supplementary Fig. 4 shows photomicrographs of immunohistochemistry staining of 4G8 and quantification of amyloid load in medial septum-diagonal band complex (MSDB; panels A and B) and caudate-putamen (CPu; panels C and D); photomicrographs of immunohistochemistry staining of GFAP and quantification of astrocytosis in MSDB (panels E and F) and CPu (panels G and H). Supplementary Fig. 5 shows photomicrographs of immunohistochemistry staining of 4G8 and quantification of amyloid load in the hindbrain (panels A and B) and cerebellum layers (panels C and D); photomicrographs of immunohistochemistry staining of GFAP and quantification of astrocytosis in the hindbrain (panels E and F) and cerebellum layers (panels G and H). The results were expressed as mean ± SEM. $^{*}p < 0.05$, $^{**}p < 0.01$, $^{***}p < 0.001$; a-as compared to 3-month-old APP^{NL-G-F} mice; b-as compared to 6-month-old APP^{NL-G-F} mice; c-as compared to C57BL/6J mice. (For interpretation of the references to color in this figure legend, the reader is referred to the Web version of this article.)

3-month-old APP^{NL-G-F} mice (Fig. 4E). No significant difference was found in between 6-, 9-, and 12-month-old APP^{NL-G-F} mice (Fig. 4E).

Immunostaining of TH revealed that TH-positive neurons in LC were decreased significantly in 9- and 12-month-old APP^{NL-G-F} mice in comparison with C57BL/6J (Fig. 5D). In comparison with 3- and 6-month-old APP^{NL-G-F} mice, a significant decrease in TH-positive neurons in LC was also found in 12-month-old APP^{NL-G-F} mice (Fig. 5D).

4. Discussion

Several mouse models for AD are available in the neuroscience research community. These models are used to test the amyloid hypothesis and to investigate the therapeutic potential of drug candidates for treating AD. Overexpression of APP is the main limitation associated with transgenic mouse models for AD, which induces phenotypic artifacts. Considering this limitation, a knock-in strategy of familial AD mutations was used to generate a new mouse model for AD, the APP^{NL-G-F}. This model carries humanized Aβ sequence, Swedish (NL), Arctic (G), and Iberian (F) mutations (Saito et al., 2014). This newly developed mouse model has gained popularity among researchers; however, the cognitive functions and biochemical alterations are not fully characterized. It is important to fully characterize the phenotype of this mouse model. In the present study, we performed various age-dependent behavioral (MWM, object recognition, FC, and general activity) tests and studied the associated biochemical alterations in the brain. Table 2 summarizes a comparative analysis in between the current findings and findings from previous studies (Hernandez et al., 2017; Masuda et al., 2016; Saito et al., 2014; Whyte et al., 2018).

4.1. Age-dependent learning and memory functions of APP^{NL-G-F}

In the present study, we found that the newly developed mouse model known as APP^{NL-G-F} showed an age-dependent impairment

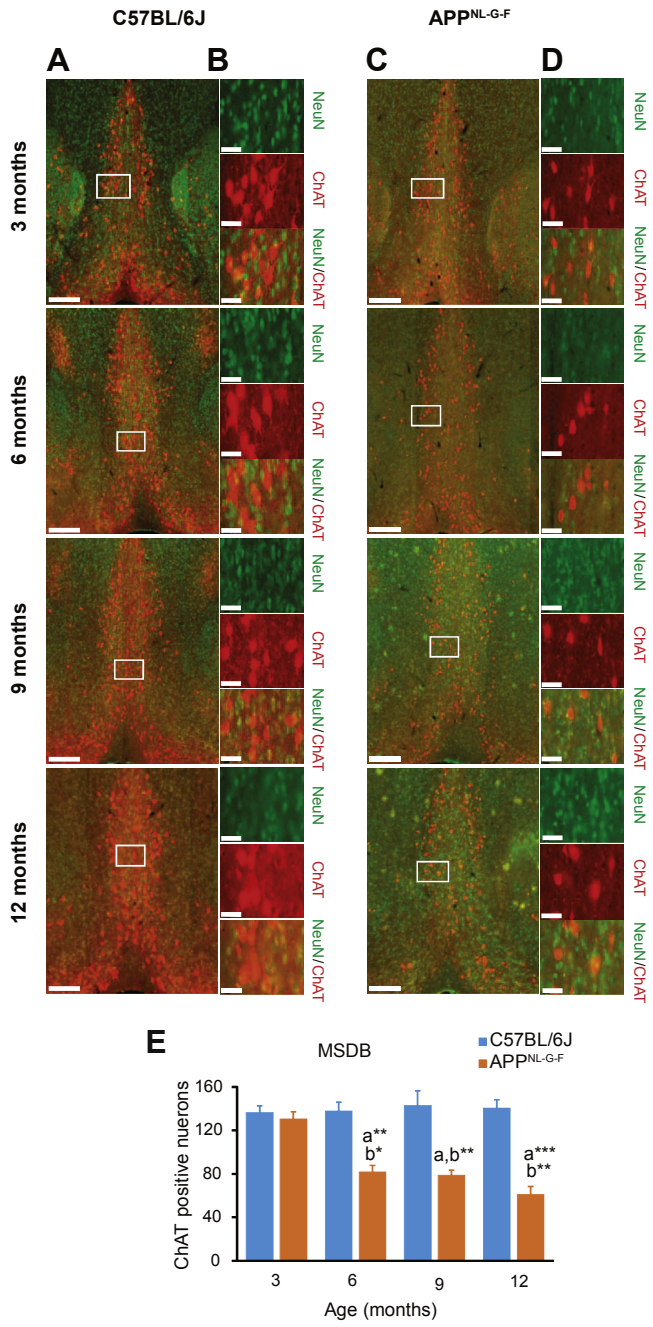

Fig. 4. Photomicrographs of immunohistochemistry staining of choline acetyltransferase (ChAT)-positive neurons in medial septum-diagonal band (MSDB) complex of the basal forebrain of C57BL/6J (panels A and B) and APP^{NL-G-F} (panels C and D) mice. ChAT: a cholinergic marker stained with monoclonal rabbit anti-ChAT antibody (red), NeuN: a neuronal marker stained with monoclonal mouse anti-NeuN antibody (green). Scale bar: 500 μm for whole sections and 50 μm for magnified sections. Panel B represents magnified images of white box in panel A and panel D represents magnified images of white box in panel C. The quantification of ChAT neurons is shown in panel E. Data are presented as mean ± SEM. $^{*}p < 0.05$, $^{**}p < 0.01$, $^{***}p < 0.001$; a-as compared to 3-month-old APP^{NL-G-F} mice; b-as compared to C57BL/6J mice. (n = 4 for C57BL/6J mice; n = 4 for APP^{NL-G-F} mice). (For interpretation of the references to color in this figure legend, the reader is referred to the Web version of this article.)

of learning and memory functions in various behavioral tests. In the MWM, APP^{NL-G-F} mice showed normal spatial learning and memory functions at the age of 3 months, which were equivalent to control mice. At the age of 6 and 9 months, APP^{NL-G-F} mice were severely impaired at spatial learning and memory as assessed with the MWM and associated classic measures of these complex cognitive processes. The difference was evidenced by a significant increase in latency to reach the platform on day 8 when compared to the control mice during the acquisition phase. Impairment in spatial memory was also observed in APP^{NL-G-F} mice indicated by no significant difference in the time spent in the target quadrant and average of other quadrants. In addition, APP^{NL-G-F} mice spent significantly less time in the target quadrant as compared to control mice. The average proximity to the platform during the probe trial was significantly higher in the APP^{NL-G-F} group when compared with the control group. Severe impairment in the learning ability of the APP^{NL-G-F} mice was observed at the age of 12 months, indicated by no significant difference in the latency to reach the platform on days 1 and 8. APP^{NL-G-F} mice showed an impairment in spatial memory in the probe test indicated by no significant difference in the time spent by APP^{NL-G-F} mice in target quadrant and average of other quadrants. The APP^{NL-G-F} mice spent significantly less time in the target quadrant as compared to control mice, showing impairment in memory. At the age of 6, 9, and 12 months, the average proximity to the platform was significantly higher in the APP^{NL-G-F} group compared to the control group, indicating an impairment in spatial memory. This is the first report which indicates age-dependent cognitive dysfunctions in APP^{NL-G-F} mice. Similar to previous experimental models for AD, APP^{NL-G-F} mice in the present study also showed an age-dependent impairment of learning and memory functions in various behavioral paradigms (Dodart et al., 2002; Hsiao et al., 1996; Mucke et al., 1994).

In the MWM, the C57BL/6J mice showed no age-dependent impairment in spatial learning and memory during acquisition training or the probe trial test. This indicates that the testing age points did not affect the learning and memory performance of control mice. It has been reported in previous studies that 12-, 13-, and 19-month-old C57BL/6J also learned this task efficiently and showed spatial memory retention in the probe trial (Wong and Brown, 2007; Yanai et al., 2018; Yin et al., 2016). However, APP^{NL-G-F} mice showed a progressive deterioration of learning and memory abilities with respect to age. The average proximity to the platform was also significantly increased at the age of 6, 9, and 12 months compared to 3 months in the APP^{NL-G-F} group. These results indicate an age-dependent impairment of spatial learning and memory functions of APP^{NL-G-F} mice. These results partially contradict previous studies (Saito et al., 2014; Whyte et al., 2018) showing no impairment of learning and memory functions in MWM at the age of 6 months. These discrepancies in the results may be due to differences in the protocol followed for MWM test in these studies. In another study, the APP^{NL-G-F} mice did not show any impairment in MWM test when they were 10–11 months old (Hernandez et al., 2018). A different protocol for MWM test and repeated behavioral measurement used in previous study may be responsible for discrepancies in the results (Hernandez et al., 2018). Moreover, in our pilot experiment, we also found that APP^{NL-G-F} mice undergoing repeated behavioural tests showed an improvement in spatial learning and memory functions in MWM when they were 12 months old (Supplementary Fig. 3). In a previous study, it has already been reported that periodic spatial learning and memory training ameliorated the impairments of cognitive functions in aged 3xTg-AD mice (Martinez-Coria et al., 2015). Therefore, in our study, we used a different cohort of mice at each testing points to rule out the positive effect of recurrent training on spatial learning and memory functions of mice.

Aversive classical conditioning processes in APP^{NL-G-F} mice in FC test was tested. The C57BL/6J mice showed intact learning and memory functions at 3, 6, 9 and 12 months. However, aversive tone and contextual conditioning was impaired in 6-, 9-, and 12-month-old APP^{NL-G-F} mice, indicating an age-dependent impairment of

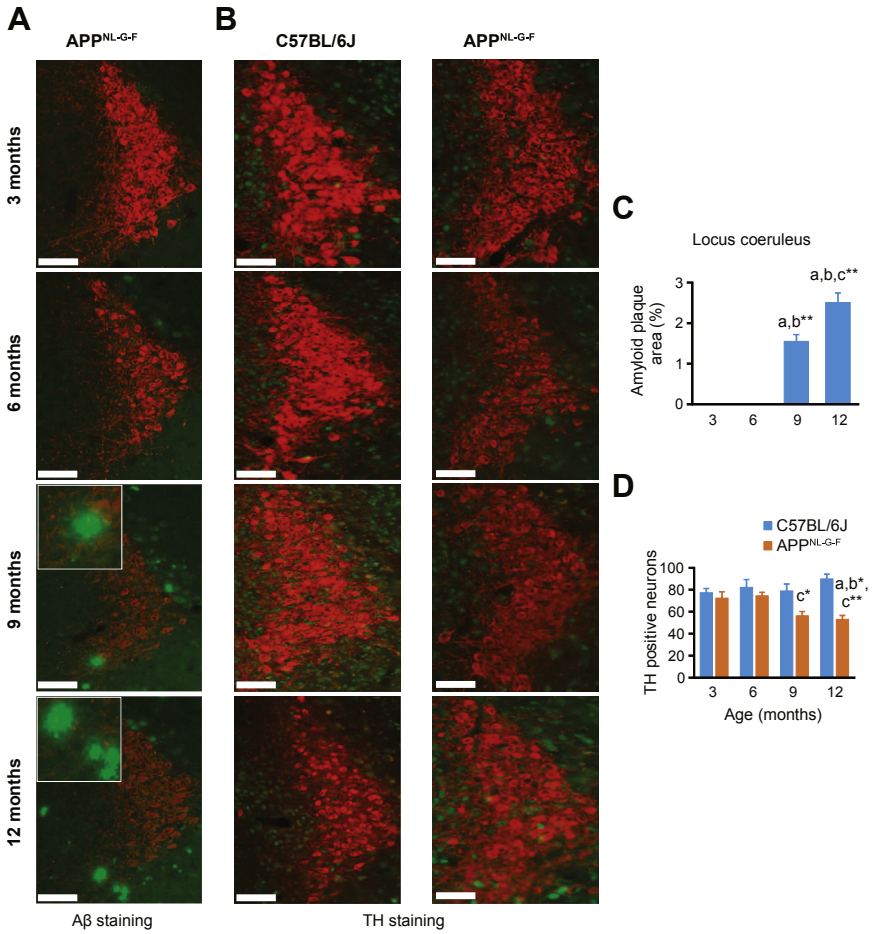

Fig. 5. (A and C) Photomicrographs of immunohistochemistry staining of 4G8 and quantification of amyloid load in locus coeruleus of APP^{NL-G-F} mice; (B and D) Photomicrographs of immunohistochemistry staining of tyrosine hydroxylase (TH)-positive neurons and quantification of TH-positive neurons in locus coeruleus of C57BL/6J and APP^{NL-G-F} mice. Amyloid plaques are stained with anti-4G8 antibody (green, panel A); TH: a noradrenergic marker stained with rabbit anti-TH antibody (red, panels A, B), NeuN: a neuronal marker stained with monoclonal mouse anti-NeuN antibody (green, panel B). Scale bar: 250 μm for whole sections. The quantification of TH neurons is shown in panel D. Data are presented as mean ± SEM. $^{*}p < 0.05$, $^{**}p < 0.01$; a-as compared to 3-month-old APP^{NL-G-F} mice; b-as compared to 6-month-old APP^{NL-G-F} mice; c-as compared to C57BL/6J mice. (n = 4 for C57BL/6J mice; n= 4 for APP^{NL-G-F} mice). (For interpretation of the references to color in this figure legend, the reader is referred to the Web version of this article.)

amygdala- and hippocampus-associated memory function. Currently, no study has reported an amygdala-associated memory impairment in this mouse model. The cued and contextual FC tests have been shown to be dependent on the amygdala and hippocampus, respectively (Phillips and LeDoux, 1992). The impaired memory function of APP^{NL-G-F} mice in these tests indicates that these brain regions are affected in this AD mouse model.

In the object recognition test, control mice showed memory retention at the age of 3, 6, 9, and 12 months. In accordance with our findings, 12-month-old C57BL/6J showed no impairment of object-associated memory in comparison to 4-month-old mice (Polydoro et al., 2009; Yang et al., 2014). In the present study, APP^{NL-G-F} mice showed no memory impairment at the age of 3 and 6 months. In a previous study also, APP^{NL-G-F} mice showed no memory impairment in the novel object recognition test at 6 months of age (Whyte et al., 2018), supporting the findings of our study. However, at the age of 9 and 12 months, APP^{NL-G-F} mice showed an impairment of memory, indicated by a significant reduction in time spent by APP^{NL-G-F} mice exploring the novel object as compared to control mice. In addition, APP^{NL-G-F} mice spent significantly less time exploring the novel object at the age of 9 and 12 months in comparison with 3 months, indicating a progressive memory impairment. The object recognition memory is thought to dependent on the perirhinal cortex circuitry, which suggests that this brain region is compromised in this AD mouse model (Antunes and Biala, 2012).

The novelty-induced behavior such as horizontal activity, vertical activity, total distance traveled, total move number, total move time, margin and center distance traveled, and rearing activity was not changed significantly in C57BL/6J and APP^{NL-G-F} mice when they were 3, 6, 9, or 12 months old, indicating that testing age points does not affect the general locomotor, exploratory, and rearing activities of APP^{NL-G-F} mice.

4.2. Age-dependent amyloid load, astrocytosis, cholinergic, and norepinephrine functions in APP^{NL-G-F} mice brain

This study is the first to investigate plaque deposition in different brain areas (MSDB complex, CPu, cortex, hippocampus, hindbrain, cerebellum, and LC) of APP^{NL-G-F} mice. Plaque formation was found in the MSDB complex, CPu, cortex, and hippocampus when mice were 6, 9, and 12 months old. Plaques were found to peak at the age of 9 months as no significant change in the plaques deposition between 9- and 12-month-old mice was found. These findings are in accordance with previous studies (Masuda et al., 2016; Saito et al., 2014; Whyte et al., 2018). This is the first report of plaque deposition in the MSDB complex, a major site for cholinergic input, and CPu. The involvement of the MSDB complex

Table 2
Differing memory performance and neuropathology between APP^{NL-G-F} mice used in our study compared with Hernandez et al. (2017), Masuda et al. (2016), Saito et al. (2014), and Whyte et al. (2018).

Behavioral & Biochemical parameters			Our study Age of mice (months)				Saito et al. Age of mice (months)					Hernandez et al. Age of mice (months)				Masuda et al. Age of mice (months)			Whyte et al. Age of mice (months)	Confirmatory/ Novel findings
			3	6	9	12	2	4	6	7	9	3-4	6-7	10-11	12	6	1st phase (8-12 M) 12	2nd phase (13-17 M) 18	6	
Behavioral tests	Morris water maze																			Novel
	Novel Object Recognition																			Novel
	Fear Conditioning																			Novel
	Y-maze																			
	Novelty Associated Locomotor Activity																			Novel
	Social Preference																			
	Elevated Plus Maze																			
	Open Field																			
	Place Preference																			
	Reversal learning																			
	Impulsivity																			
	Attention																			
	Delay-discounting task (Compulsivity)																			
	Place Avoidance Memory																			
Biochemical markers	Aβ plaques	Cortex																		Confirmatory
		MSDB																		Novel
		CPu																		Novel
		HP																		Confirmatory
		HB																		Novel
		LC																		Novel
		CB																		Novel
		CC																		
		BS																		
		AC																		
	Astrocytosis (GFAP)	Cortex																		Confirmatory
		MSDB																		Novel
		CPu																		Novel
		HP																		Confirmatory
		HB																		Novel
		CB																		Novel
	Microgliosis (IBA1)	Cortex																		
	ChAT	MSDB																		Novel
	TH	LC																		Novel
	Synaptophysin	Brain																		
	PSD95	Brain																		

Not done | Same as control | Increased from control | Decreased from control

White cells represent time points where no data are available for the respective behavior and biochemical markers, light gray cells represent no change compared to controls, black cells represent increases compared to control, dark gray cells represent decreases compared to control.
Key: MSDB, medial septum-diagonal band; CPu, caudate-putamen; HP, hippocampus; HB, hindbrain; LC, locus coeruleus; CB, cerebellum; CC, corpus callosum, brainstem; AC, anterior commissure; ChAT, choline acetyltransferase; TH, Tyrosine hydroxylase.

and CPu in learning and memory processes is well documented (Baxter et al., 2013; De Simoni et al., 2018; Givens and Olton, 1990; Hall and Savage, 2016; Knox and Keller, 2016; Okada et al., 2015; Roland et al., 2014; Setlow and McGaugh, 1999; Xu et al., 2012). In addition, 9- and 12-month-old APP^{NL-G-F} mice showed plaque deposition in the hindbrain, cerebellum, and LC, and the involvement of these brain regions in various cognitive and motor functions is also well known. At this time, there has been no report of plaque deposition in these brain areas. However, we did not find plaques deposition in the 3-month-old the APP^{NL-G-F} mice brain.

The MSDB complex influences various hippocampus-dependent cognitive functions, including learning and memory through projections from cholinergic, GABAergic, and glutamatergic neurons (Amaral and Kurz, 1985). Lesions or inactivation of MSDB complex causes hippocampal-dependent learning and memory impairments (Craig et al., 2011; Givens and Olton, 1990). In the present study, a decrease in ChAT-positive neurons in the MSDB complex in 6-, 9-, and 12-month-old APP^{NL-G-F} mice was found. One hypothesis is that in the case of the APP^{NL-G-F} mice, amyloid plaque deposition in this brain region may lead to neuroinflammation and, collectively, plaques and inflammation may result in cholinergic dysfunction, which finally progresses into cognitive impairment.

The LC, a primary site for NE synthesis, is one of the earliest brain regions affected by AD, and neurodegeneration in the LC is a well-known characteristic of AD pathology (Daulatzai, 2016; Kelly et al., 2017; Leanza et al., 2018). The LC projects to all brain regions important for learning and memory, such as the hippocampus, entorhinal cortex, prefrontal cortex, and amygdala (Ross et al., 2015). The reduction in cortical NE levels has been associated with cognitive impairment (Matthews et al., 2002). Moreover, low levels of NE in the brain enhanced the Aβ plaque burden in transgenic mouse models of AD (Kalinin et al., 2007). The degeneration of TH-positive neuron and loss of NE transporter in the LC has been reported in APP/PS1 transgenic mouse model (Liu et al., 2013). In addition, mice obtained after crossing of APP/PS1 with dopamine β-hydroxylase knockout (DBH-/-) mice showed severe impairment in water maze performance, indicating involvement of NE in AD pathology (Hammerschmidt et al., 2013). Similarly, the results of the present study indicate the loss of TH-positive neurons in the LC in 9- and 12-month-old APP^{NL-G-F} mice, and the loss of TH neurons may also be responsible for the impairment of learning and memory functions of this AD mouse model.

The involvement of inflammation in AD pathology is well studied, and several inflammatory markers have been detected in AD brains (Akiyama et al., 2000). Accumulation of both astrocytes and microglia around the plaques has been reported in previous study (Nilsson et al., 2014). Increased astrocytosis in the different brain regions of APP^{NL-G-F} mice was also found in the present study,

and these findings are in accordance with previous studies (Masuda et al., 2016; Saito et al., 2014). In previous studies, astrocytosis and microgliosis, an indicator of neuroinflammation, have also been reported (Masuda et al., 2016; Saito et al., 2014).

5. Conclusion

The findings of the present study indicate that the APP^{NL-G-F} mice showed learning and memory impairment in various behavioral paradigms, as discussed. This AD mouse model also showed age-dependent deposition of amyloid plaque and increased astrocytosis in different brain areas. In addition, APP^{NL-G-F} mice showed both cholinergic and NE dysfunction. Together, the results of the present study support the suitability of APP^{NL-G-F} mice with no overexpression of APP as an important improvement in available AD mouse models. APP^{NL-G-F} mice will be very useful to investigate the involvement of various risk factors in AD pathophysiology and to screen various drug candidates for therapeutic potential. Further studies are required to address the questions related to this AD mouse model: (1) Is there any difference between heterozygous and homozygous APP^{NL-G-F} mice with respect to AD pathology and cognitive functions in age-dependent manner? (2) Are various neuronal networks impaired in this AD mouse model and what are they? (3) Is there any neurodegeneration or neuronal loss in this mouse model?

Disclosure

The authors have no actual or potential conflicts of interest.

Acknowledgements

This work was supported by Natural Sciences and Engineering Research Council of Canada, Canada Discovery Grant #40352, #06347, and #03857 to MHM, RJM, BLM, and RJS, respectively, Alberta Innovates (MHM and BLM), Alberta Alzheimer Research Program (MHM), Alzheimer Society of Canada (MHM and RJM), Alberta Prion Research Institute (MHM and RJS), and Canadian Institute for Health Research (MHM, BLM, RJM, and RJS). The authors thank Dr Takashi Saito and Prof. Takaomi C Saido from "Laboratory for Proteolytic Neuroscience RIKEN Center for Brain Science, Wako-shi, Saitama, Japan" for providing the $APP^{NL-G-F/NL-G-F}$ mice as a gift. The authors also thank Di Shao and Behroo Mirza Agha for animal breeding.

Authors' contributions: MHM, RJM, and RJS designed the experiments and supervised the study. JM and SGL performed the behavioral experiments and analyzed the behavioral data. VL performed the immunohistochemistry and fluorescent imaging assays, and JM analyzed the ex vivo imaging data. JM and MHM wrote the article, which all authors commented on and edited.

Appendix A. Supplementary data

Supplementary data to this article can be found online at https://doi.org/10.1016/j.neurobiolaging.2018.10.026.

References

Akiyama, H., Barger, S., Barnum, S., Bradt, B., Bauer, J., Cole, G.M., Cooper, N.R., Eikelenboom, P., Emmerling, M., Fiebich, B.L., Finch, C.E., Frautschy, S., Griffin, W.S., Hampel, H., Hull, M., Landreth, G., Lue, L., Mrak, R., Mackenzie, I.R., McGeer, P.L., O'Banion, M.K., Pachter, J., Pasinetti, G., Plata-Salaman, C., Rogers, J., Rydel, R., Shen, Y., Streit, W., Strohmeyer, R., Tooyoma, I., Van Muiswinkel, F.L., Veerhuis, R., Walker, D., Webster, S., Wegrzyniak, B., Wenk, G., Wyss-Coray, T., 2000. Inflammation and Alzheimer's disease. Neurobiol. Aging 21, 383–421.

Amaral, D.G., Kurz, J., 1985. An analysis of the origins of the cholinergic and non-cholinergic septal projections to the hippocampal formation of the rat. J. Comp. Neurol. 240, 37–59.

Antunes, M., Biala, G., 2012. The novel object recognition memory: neurobiology, test procedure, and its modifications. Cogn. Process. 13, 93–110.

Bateman, R.J., Xiong, C., Benzinger, T.L.S., Fagan, A.M., Goate, A., Fox, N.C., Marcus, D.S., Cairns, N.J., Xie, X., Blazey, T.M., Holtzman, D.M., Santacruz, A., Buckles, V., Oliver, A., Moulder, K., Aisen, P.S., Ghetti, B., Klunk, W.E., McDade, E., Martins, R.N., Masters, C.L., Mayeux, R., Ringman, J.M., Rossor, M.N., Schofield, P.R., Sperling, R.A., Salloway, S., Morris, J.C., Dominantly Inherited Alzheimer Network, 2012. Clinical and biomarker changes in dominantly inherited Alzheimer's disease. N. Engl. J. Med. 367, 795–804.

Baxter, M.G., Bucci, D.J., Gorman, L.K., Wiley, R.G., Gallagher, M., 2013. Selective immunotoxic lesions of basal forebrain cholinergic cells: effects on learning and memory in rats. Behav. Neurosci. 127, 619–627.

Cavanaugh, S.E., Pippin, J.J., Barnard, N.D., 2014. Animal models of Alzheimer disease: historical pitfalls and a path forward. ALTEX 31, 279–302.

Craig, L.A., Hong, N.S., McDonald, R.J., 2011. Revisiting the cholinergic hypothesis in the development of Alzheimer's disease. Neurosci. Biobehav. Rev. 35, 1397–1409.

Daulatzai, M.A., 2016. Dysfunctional sensory Modalities, locus coeruleus, and basal forebrain: early Determinants that Promote Neuropathogenesis of cognitive and memory decline and Alzheimer's disease. Neurotox Res. 30, 295–337.

De Simoni, S., Jenkins, P.O., Bourke, N.J., Fleminger, J.J., Hellyer, P.J., Jolly, A.E., Patel, M.C., Cole, J.H., Leech, R., Sharp, D.J., 2018. Altered caudate connectivity is associated with executive dysfunction after traumatic brain injury. Brain 141, 148–164.

de Vugt, M.E., Stevens, F., Aalten, P., Lousberg, R., Jaspers, N., Verhey, F.R., 2005. A prospective study of the effects of behavioral symptoms on the institutionalization of patients with dementia. Int. Psychogeriatr. 17, 577–589.

Dodart, J.C., Bales, K.R., Gannon, K.S., Greene, S.J., DeMattos, R.B., Mathis, C., DeLong, C.A., Wu, S., Wu, X., Holtzman, D.M., Paul, S.M., 2002. Immunization reverses memory deficits without reducing brain Abeta burden in Alzheimer's disease model. Nat. Neurosci. 5, 452–457.

Ettcheto, M., Abad, S., Petrov, D., Pedrós, I., Busquets, O., Sánchez-López, E., Casadesús, G., Beas-Zarate, C., Carro, E., Auladell, C., Olloquequi, J., Pallàs, M., Folch, J., Camins, A., 2018. Early preclinical changes in hippocampal CREB-Binding protein expression in a mouse model of familial Alzheimer's disease. Mol. Neurobiol. 55, 4885–4895.

Ettcheto, M., Sánchez-López, E., Pons, L., Busquets, O., Olloquequi, J., Beas-Zarate, C., Pallas, M., García, M.L., Auladell, C., Folch, J., Camins, A., 2017. Dexibuprofen prevents neurodegeneration and cognitive decline in APPswe/PS1dE9 through multiple signaling pathways. Redox Biol. 13, 345–352.

Ferri, C.P., Ames, D., Prince, M., 10/66 Dementia Research Group, 2004. Behavioral and psychological symptoms of dementia in developing countries. Int. Psychogeriatr. 16, 441–459.

Francis, P.T., Palmer, A.M., Snape, M., Wilcock, G.K., 1999. The cholinergic hypothesis of Alzheimer's disease: a review of progress. J. Neurol. Neurosurg. Psychiatry 66, 137–147.

Frölich, L., 2002. The cholinergic pathology in Alzheimer's disease—discrepancies between clinical experience and pathophysiological findings. J. Neural Transm. (vienna) 109, 1003–1013.

Gidyk, D.C., Deibel, S.H., Hong, N.S., McDonald, R.J., 2015. Barriers to developing a valid rodent model of Alzheimer's disease: from behavioral analysis to etiological mechanisms. Front. Neurosci. 9, 245.

Gil-Bea, F.J., García-Alloza, M., Domínguez, J., Marcos, B., Ramírez, M.J., 2005. Evaluation of cholinergic markers in Alzheimer's disease and in a model of cholinergic deficit. Neurosci. Lett. 375, 37–41.

Givens, B.S., Olton, D.S., 1990. Cholinergic and GABAergic modulation of medial septal area: effect on working memory. Behav. Neurosci. 104, 849–855.

Hall, A.M., Roberson, E.D., 2012. Mouse models of Alzheimer's disease. Brain Res. Bull. 88, 3–12.

Hall, J.M., Savage, L.M., 2016. Exercise leads to the re-emergence of the cholinergic/nestin neuronal phenotype within the medial septum/diagonal band and subsequent rescue of both hippocampal ACh efflux and spatial behavior. Exp. Neurol. 278, 62–75.

Hammerschmidt, T., Kummer, M.P., Terwel, D., Martinez, A., Gorji, A., Pape, H.C., Rommelfanger, K.S., Schroeder, J.P., Stoll, M., Schultze, J., Weinshenker, D., Heneka, M.T., 2013. Selective loss of noradrenaline exacerbates early cognitive dysfunction and synaptic deficits in APP/PS1 mice. Biol. Psychiatry 73, 454–463.

Hardy, J., Selkoe, D.J., 2002. The amyloid hypothesis of Alzheimer's disease: progress and problems on the road to therapeutics. Science 297, 353–356.

Hernandez, A.L., Shah, D., Craessaerts, K., Saido, T., Saito, T., De Strooper, B., Van der Linden, A., D'Hooge, R., 2017. Subtle behavioral changes and increased prefrontal-hippocampal network synchronicity in APP(NL-G-F) mice before prominent plaque deposition. Behav. Brain Res. [Epub ahead of print].

Hsiao, K., Chapman, P., Nilsen, S., Eckman, C., Harigaya, Y., Younkin, S., Yang, F., Cole, G., 1996. Correlative memory deficits, Abeta elevation, and amyloid plaques in transgenic mice. Science 274, 99–102.

Kalinin, S., Gavrilyuk, V., Polak, P.E., Vasser, R., Zhao, J., Heneka, M.T., Feinstein, D.L., 2007. Noradrenaline deficiency in brain increases beta-amyloid plaque burden in an animal model of Alzheimer's disease. Neurobiol. Aging 28, 1206–1214.

Kee, N., Teixeira, C.M., Wang, A.H., Frankland, P.W., 2007. Preferential incorporation of adult-generated granule cells into spatial memory networks in the dentate gyrus. Nat. Neurosci. 10, 355–362.

Kelly, S.C., He, B., Perez, S.E., Ginsberg, S.D., Mufson, E.J., Counts, S.E., 2017. Locus coeruleus cellular and molecular pathology during the progression of Alzheimer's disease. Acta Neuropathol. Commun. 5, 8.

Knox, D., Keller, S.M., 2016. Cholinergic neuronal lesions in the medial septum and vertical limb of the diagonal bands of Broca induce contextual fear memory generalization and impair acquisition of fear extinction. Hippocampus 26, 718–726.

Leanza, G., Gulino, R., Zorec, R., 2018. Noradrenergic hypothesis Linking neurodegeneration-based cognitive decline and Astroglia. Front. Mol. Neurosci. 11, 254.

Li, Y., 2013. Establishment of experimental models for Alzheimer's disease research. Int. J. Neurosci. 123, 823–831.

Li, X., Bao, X., Wang, R., 2016. Experimental models of Alzheimer's disease for deciphering the pathogenesis and therapeutic screening (Review). Int. J. Mol. Med. 37, 271–283.

Liu, L., Luo, S., Zeng, L., Wang, W., Yuan, L., Jian, X., 2013. Degenerative alterations in noradrenergic neurons of the locus coeruleus in Alzheimer's disease. Neural Regen. Res. 8, 2249–2255.

Martinez-Coria, H., Yeung, S.T., Ager, R.R., Rodriguez-Ortiz, C.J., Baglietto-Vargas, D., LaFerla, F.M., 2015. Repeated cognitive stimulation alleviates memory impairments in an Alzheimer's disease mouse model. Brain Res. Bull 117, 10–15.

Masuda, A., Kobayashi, Y., Kogo, N., Saito, T., Saido, T.C., Itohara, S., 2016. Cognitive deficits in single App knock-in mouse models. Neurobiol. Learn. Mem. 135, 73–82.

Matthews, K.L., Chen, C.P., Esiri, M.M., Keene, J., Minger, S.L., Francis, P.T., 2002. Noradrenergic changes, aggressive behavior, and cognition in patients with dementia. Biol. Psychiatry 51, 407–416.

McDonald, R.J., 2002. Multiple combinations of co-factors produce variants of age-related cognitive decline: a theory. Can. J. Exp. Psychol. 56, 221–239.

McDonald, R.J., Craig, L.A., Hong, N.S., 2010. The etiology of age-related dementia is more complicated than we think. Behav. Brain Res. 214, 3–11.

Mehla, J., Deibel, S.H., Faraji, J., Saito, T., Saido, T.C., Mohajerani, M.H., McDonald, R.J., 2018a. Looking beyond the standard version of the Morris water task in the assessment of mouse models of cognitive deficits. Hippocampus. https://doi.org/10.1002/hipo.22999 [Epub ahead of print].

Mehla, J., Lacoursiere, S., Stuart, E., McDonald, R.J., Mohajerani, M.H., 2018b. Gradual Cerebral hypoperfusion Impairs fear conditioning and object recognition learning and memory in mice: potential roles of neurodegeneration and cholinergic dysfunction. J. Alzheimers Dis. 61, 283–293.

Mucke, L., Masliah, E., Johnson, W.B., Ruppe, M.D., Alford, M., Rockenstein, E.M., Forss-Petter, S., Pietropaolo, M., Mallory, M., Abraham, C.R., 1994. Synaptotrophic effects of human amyloid beta protein precursors in the cortex of transgenic mice. Brain Res. 666, 151–167.

Nilsson, P., Saito, T., Saido, T.C., 2014. New mouse model of Alzheimer's. ACS Chem. Neurosci. 5, 499–502.

Okada, K., Nishizawa, K., Kobayashi, T., Sakata, S., Kobayashi, K., 2015. Distinct roles of basal forebrain cholinergic neurons in spatial and object recognition memory. Sci. Rep. 5, 13158.

Peters, D.G., Pollack, A.N., Cheng, K.C., Sun, D., Saido, T., Haaf, M.P., Yang, Q.X., Connor, J.R., Meadowcroft, M.D., 2018. Dietary lipophilic iron alters amyloidogenesis and microglial morphology in Alzheimer's disease knock-in APP mice. Metallomics 10, 426–443.

Phillips, R.G., LeDoux, J.E., 1992. Differential contribution of amygdala and hippocampus to cued and contextual fear conditioning. Behav. Neurosci. 106, 274–285.

Polydoro, M., Acker, C.M., Duff, K., Castillo, P.E., Davies, P., 2009. Age-dependent impairment of cognitive and synaptic function in the htau mouse model of tau pathology. J. Neurosci. 29, 10741–107449.

Roland, J.J., Stewart, A.L., Janke, K.L., Gielow, M.R., Kostek, J.A., Savage, L.M., Servatius, R.J., Pang, K.C., 2014. Medial septum-diagonal band of Broca (MSDB) GABAergic regulation of hippocampal acetylcholine efflux is dependent on cognitive demands. J. Neurosci. 34, 506–514.

Ross, J.A., McGonigle, P., Van Bockstaele, E.J., 2015. Locus Coeruleus, norepinephrine and Aβ peptides in Alzheimer's disease. Neurobiol. Stress 2, 73–84.

Saito, T., Matsuba, Y., Mihira, N., Takano, J., Nilsson, P., Itohara, S., Iwata, N., Saido, T.C., 2014. Single App knock-in mouse models of Alzheimer's disease. Nat. Neurosci. 17, 661–663.

Santos, C.Y., Snyder, P.J., Wu, W.C., Zhang, M., Echeverria, A., Alber, J., 2017. Pathophysiologic relationship between Alzheimer's disease, cerebrovascular disease, and cardiovascular risk: a review and synthesis. Alzheimers Dement. (Amst) 7, 69–87.

Sasaguri, H., Nilsson, P., Hashimoto, S., Nagata, K., Saito, T., De Strooper, B., Hardy, J., Vassar, R., Winblad, B., Saido, T.C., 2017. APP mouse models for Alzheimer's disease preclinical studies. EMBO J. 36, 2473–2487.

Sberna, G., Sáez-Valero, J., Li, Q.X., Czech, C., Beyreuther, K., Masters, C.L., McLean, C.A., Small, D.H., 1998. Acetylcholinesterase is increased in the brains of transgenic mice expressing the C-terminal fragment (CT100) of the beta-amyloid protein precursor of Alzheimer's disease. J. Neurochem. 71, 723–731.

Setlow, B., McGaugh, J.L., 1999. Involvement of the posteroventral caudate-putamen in memory consolidation in the Morris water maze. Neurobiol. Learn. Mem. 71, 240–247.

Vogel-Ciernia, A., Wood, M.A., 2014. Examining object location and object recognition memory in mice. Curr. Protoc. Neurosci. 69, 1–17.

Whyte, L.S., Hemsley, K.M., Lau, A.A., Hassiotis, S., Saito, T., Saido, T.C., Hopwood, J.J., Sargeant, T.J., 2018. Reduction in open field activity in the absence of memory deficits in the App(NL-G-F) knock-in mouse model of Alzheimer's disease. Behav. Brain Res. 336, 177–181.

Wiltgen, B.J., Sanders, M.J., Ferguson, C., Homanics, G.E., Fanselow, M.S., 2005. Trace fear conditioning is enhanced in mice lacking the delta subunit of the GABAA receptor. Learn. Mem. 12, 327–333.

Wong, A.A., Brown, R.E., 2007. Age-related changes in visual acuity, learning and memory in C57BL/6J and DBA/2J mice. Neurobiol. Aging 28, 1577–1593.

Xu, H., Yang, H.J., Rose, G.M., 2012. Chronic haloperidol-induced spatial memory deficits accompany the upregulation of D(1) and D(2) receptors in the caudate putamen of C57BL/6 mouse. Life Sci. 91, 322–328.

Yanai, S., Ito, H., Endo, S., 2018. Long-term cilostazol administration prevents age-related decline of hippocampus-dependent memory in mice. Neuropharmacology 129, 57–68.

Yang, L., Zhang, J., Zheng, K., Shen, H., Chen, X., 2014. Long-term ginsenoside Rg1 supplementation improves age-related cognitive decline by promoting synaptic plasticity associated protein expression in C57BL/6J mice. J. Gerontol. A. Biol. Sci. Med. Sci. 69, 282–294.

Yin, R., Yin, K., Guo, Z., Zhang, Z., Chen, L., Cao, L., Li, Y., Wei, Y., Fu, X., Shi, X., 2016. Protective effects of Colivelin against Alzheimer's disease in a PDAPP mouse model. Cell Physiol. Biochem. 38, 1138–1146.

Zuloaga, K.L., Johnson, L.A., Roese, N.E., Marzulla, T., Zhang, W., Nie, X., Alkayed, F.N., Hong, C., Grafe, M.R., Pike, M.M., Raber, J., Alkayed, N.J., 2016. High fat diet-induced diabetes in mice exacerbates cognitive deficit due to chronic hypoperfusion. J. Cereb. Blood Flow. Metab. 36, 1257–1270.